Unified model predictive control method of automated vehicles for lane-changing and lane-keeping maneuvers

Liu, Wei; Song, Li; Dong, Yongqi; Zhang, Xuequan; Xu, Liangjie

DOI
10.1080/15472450.2025.2479235

Publication date
2025

Document Version
Final published version

Published in
Journal of Intelligent Transportation Systems: technology, planning, and operations

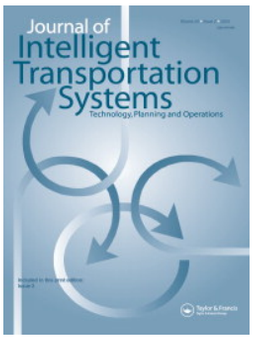

Taylor & Francis
Taylor & Francis Group

Journal of Intelligent Transportation Systems
Technology, Planning, and Operations

ISSN: (Print) (Online) Journal homepage: www.tandfonline.com/journals/gits20

Unified model predictive control method of automated vehicles for lane-changing and lane-keeping maneuvers

Wei Liu, Li Song, Yongqi Dong, Xuequan Zhang & Liangjie Xu

To cite this article: Wei Liu, Li Song, Yongqi Dong, Xuequan Zhang & Liangjie Xu (20 Mar 2025): Unified model predictive control method of automated vehicles for lane-changing and lane-keeping maneuvers, Journal of Intelligent Transportation Systems, DOI: 10.1080/15472450.2025.2479235

To link to this article: https://doi.org/10.1080/15472450.2025.2479235

JOURNAL OF INTELLIGENT TRANSPORTATION SYSTEMS
https://doi.org/10.1080/15472450.2025.2479235

Unified model predictive control method of automated vehicles for lane-changing and lane-keeping maneuvers

Wei Liu[a], Li Song[a], Yongqi Dong[b], Xuequan Zhang[a], and Liangjie Xu[a]

[a]School of Transportation and Logistics Engineering, Wuhan University of Technology, Wuhan, China; [b]Department of Transport and Planning, Faculty of Civil Engineering and Geosciences, Delft University of Technology, Delft, The Netherlands

ABSTRACT

This paper investigates the motion control of automated vehicles for both lane-changing and lane-keeping maneuvers. This research is critical because lane keeping and lane changing, which need to be integrated into a unified control system, are still two fundamental control problems on the way to developing the highly automated vehicle. In addition, environment perception, which is highly coupled with motion control, should be introduced into the control loop. A further challenge is to solve the complex optimization problem with constraints of vehicle dynamics and full-dimensional collision avoidance. To solve these issues, this paper proposes a unified model predictive control method that can seamlessly handle lane-keeping and lane-changing maneuvers. The control problem adopts three reference generation approaches to get the perception of the traffic environment involved. Further, a rough-plan-and-fine-check strategy is utilized to reduce the complexity of solving the proposed unified model predictive control problem with constraints of collision avoidance. The proposed method has been implemented on the PreScan-MATLAB/Simulink joint simulation platform, where its performance of lane keeping and lane changing has been evaluated in different driving scenarios. Simulation results verify the capabilities of the proposed method.

ARTICLE HISTORY
Received 16 May 2023
Revised 10 March 2025
Accepted 10 March 2025

KEYWORDS
automated vehicles; lane changing; lane keeping; model predictive control

1. Introduction

Automated vehicles are growing rapidly to participate in the Intelligent Transportation System (ITS) with the potential to improve traffic safety and mitigate traffic congestion (Cui et al., 2021; Marcano et al., 2020; Moradloo et al., 2025; Wang et al., 2014; Yang et al., 2018). However, it is undeniable that there are still lots of challenges that need to be overcome before they become common participants in future transportation systems.

As lane keeping and lane changing are two basic categories of driving behaviors when people drive vehicles on a structured road (Xie et al., 2019; Hu et al., 2020; Hu et al., 2019; Chen & Huang, 2017), numerous works have been done to contribute to the automated lane-keeping and lane-changing methods. Lane-keeping controllers are designed to keep the vehicle within its lane while maintaining the speed and avoiding collisions automatically (Li et al., 2021; Liang et al., 2021) and the lane-changing controllers are able to guide the automated vehicle move to the adjacent lane smoothly (Do et al., 2017; Suh & An, 2024; Yu et al., 2018).

Lane keeping and lane changing are still two essential control problems of automated vehicles (Vechione & Cheu, 2022). However, as in the above-mentioned literature and other state-of-the-art works, these two driving behaviors are studied separately with different methods. In addition, behavioral decisions on lane changing or lane keeping should be made before trajectory or path planning and motion control (Gonzalez et al., 2016; Marti et al., 2019; Xu et al., 2020). Fully or highly automated vehicles need to be deployed with control modules that are capable of automatic lane keeping and lane changing and have the functionality to switch from one to another seamlessly. Hence, it is in great need to develop control methods that can cope with lane keeping and lane changing simultaneously. Should the automated vehicle get equipped with such a controller, there will be no need to decide to keep in the current lane or change to another lane and consequently plan the corresponding path or trajectory by using different methods, which will make the automated driving system much simpler.

CONTACT Xuequan Zhang xqzhang@whut.edu.cn School of Transportation and Logistics Engineering, Wuhan University of Technology, Wuhan, China

The perception system and the control system are two general subsystems in the overall automated driving system (Li & Wang, 2007; Fu et al., 2021; Hu et al., 2021). The former one obtains the information describing the traffic environment, the state of the ego vehicle, and other vehicles by heavily relying on on-board sensors, such as cameras, LiDARs, and radars (Marti et al., 2019). The general control system of the automated vehicle consists of route planning, behavioral decision making, motion planning, and local feedback control (Gong et al., 2016; Paden et al., 2016). However, most of the related works only focus on the planning or control task of lane changing or lane keeping individually in a specific driving scenario. The overall control system would be organized with a cumbersome hierarchical structure to handle the continuous and complex driving process. Hence, there is considerable potential for the development of a compact control system by comprehensively involving the last three modules in a unified automatic lane-keeping and lane-changing control method.

Moreover, the connection between the perception system and the driving control system of automated vehicles has not been fully investigated yet. In a cycle of the information flow, the information captured by the perception system determines the control commands generated by the control system, and then the state of the ego vehicle altered by the control commands affects the information that would be obtained by the perception system. That these two systems depend on each other makes the overall automated driving system very complicated. It might be too ideal to assume that the environment is always static during the whole control period or the mapping from the traffic environment to the information obtained is stable when the ego vehicle and the environment are at different states, for instance in Liu et al. (2017). Therefore, it is appealing to develop a closed control loop that can take the perception of the environment into consideration.

The vehicle dynamics model is suitable for the accurate motion control of automated vehicles and considering multiple dynamic constraints at the same time, but it is more complex than the vehicle kinematics model. Due to the inherent capability of explicit multi-constraint handling for multiple-input and multiple-output systems, model predictive control has been widely used for the motion control of complex vehicle dynamics systems (Arrigoni et al., 2022; Falcone et al., 2007; Gao et al., 2014; Liu & Li, 2018; Rasekhipour et al., 2017). The model predictive control problem of automated vehicles for various motion control is usually transformed into a constrained optimization problem (Liu & Li, 2019; Zhai et al., 2022; Zhang et al., 2022; Zhao et al., 2022). However, it is tough to solve the complex optimization problem with constraints of vehicle dynamics and full-dimensional collision avoidance.

To address the above challenges and make the control system of automated vehicles simpler, more flexible, and more capable of dealing with various driving scenarios, we would like to propose a unified control method for lane keeping and lane changing within the framework of model predictive control. The main contributions of this work are as follows.

First, this paper proposes a method that can seamlessly solve the control problems of lane keeping and lane changing without switching from one to another, which eliminates the boundary between these two driving maneuvers and simplifies the control system of automated vehicles. Originating from the idea that lane changing and lane keeping are two different behaviors classified by human drivers but could be treated the same from the perspective of computers, this method makes automated vehicles more like machines rather than human-driven vehicles.

Second, this paper narrows the gap between the perception system and the control system of the automated vehicle by using reference generation methods, which can diminish the impact of the perception errors on the control of the trajectory tracking. Furthermore, the unified model predictive control method does not require a sophisticated path or trajectory planning method in advance. Involving the output of the perception system in the control loop, this method formulates a closed-loop control system for automated vehicles within a dynamic traffic environment.

The rest of this paper is organized as follows. Section 2 formulates the general control problem of automated vehicles driving on the structural road. Section 3 describes the proposed unified model predictive control method for lane keeping and lane changing in detail. Simulations and results under different driving scenarios are discussed in Section 4. Finally, Section 5 briefly concludes this paper.

2. Problem formulation

In this section, a generic control scheme of automated vehicles for lane changing and lane keeping is formulated.

2.1. Overall formulation

The overall structure of the automated driving system for lane change and lane keeping is introduced in

Figure 1, where the traffic environment, the vehicle dynamics, and the control system form a closed loop. The ego vehicle is a part of the traffic, and at the same time interacts with others in the traffic. The tire-road interaction is one of the direct interactions between the vehicle and the traffic environment, while the aerodynamics are not explicitly considered in this paper. The sensors detect the physical parameters of interest in the traffic environment, such as color and distance, and then provide the perception system with the digital signals that can be further processed into structured data representing objects or lane lines.

It is assumed that the automated vehicle is equipped with a decision-making module that provides a desired maneuver request, e.g., keeping in the current lane or changing to the left lane. The dashed rectangle in Figure 1 highlights the control scheme consisting of two modules for the lane-changing and lane-keeping maneuvers. The upper control module generates the steering angle and acceleration, while the lower module computes the throttle and the brake based on the acceleration requirement. That the hierarchical two-module control structure separates the general dynamics of vehicle motions and the complex dynamics of tires simplifies the overall dynamics of the control system, but still preserves the adequate ability to control the automated vehicle at a high speed.

The upper control module, namely the lane change/keeping control, which is one of the most important parts of the proposed control scheme, is formulated as an optimal control problem within the framework of model predictive control. It is able to solve the motion control problem for lane keeping or lane changing in the same way without changing its formation, no matter which driving maneuver is required. The vehicle state variable is denoted as $\boldsymbol{x} \in \mathbb{R}^{n_x}$, and the control variable is denoted as $\boldsymbol{u} \in \mathbb{R}^{n_u}$. The lane change/keeping control scheme is written as

$$\min_{\boldsymbol{u}(t)} \int_{t=0}^{T_p} J(\boldsymbol{x}(t), \boldsymbol{u}(t), \boldsymbol{r}(t)), \tag{1a}$$

$$\text{s.t. } \dot{\boldsymbol{x}}(t) = f_0(\boldsymbol{x}(t), \boldsymbol{u}(t)), t \in [0, T_p]; \tag{1b}$$

$$\boldsymbol{x}_{\min} \preceq \boldsymbol{x}(t) \preceq \boldsymbol{x}_{\max}, t \in [0, T_p]; \tag{1c}$$

$$\boldsymbol{u}_{\min} \preceq \boldsymbol{u}(t) \preceq \boldsymbol{u}_{\max}, t \in [0, T_p]; \tag{1d}$$

$$\mathcal{E}(\boldsymbol{x}(t)) \subset \mathcal{F}(t), t \in [0, T_p]. \tag{1e}$$

Herein, T_p is the length of the prediction horizon in time, J is the cost function to be minimized, $\boldsymbol{r}(t)$ is the reference trajectory that depends on the traffic environment. The function $f_0 : \mathbb{R}^{n_x} \times \mathbb{R}^{n_u} \to \mathbb{R}^{n_x}$ describes the vehicle dynamics. $[\boldsymbol{x}_{\min}, \boldsymbol{x}_{\max}]$ and $[\boldsymbol{u}_{\min}, \boldsymbol{u}_{\max}]$ denote the limitations of the vehicle state and control, respectively. $\mathcal{E}(\cdot) : \mathbb{R}^{n_x} \to \mathbb{R}^2$ is a mapping from the vehicle state to the space occupied by the controlled vehicle in the horizontal plane. $\mathcal{F} \subset \mathbb{R}^2$ represents the free space where the vehicle does not collide with other objects. The details behind the aforementioned abstract symbols will be explained in the remainder of this section.

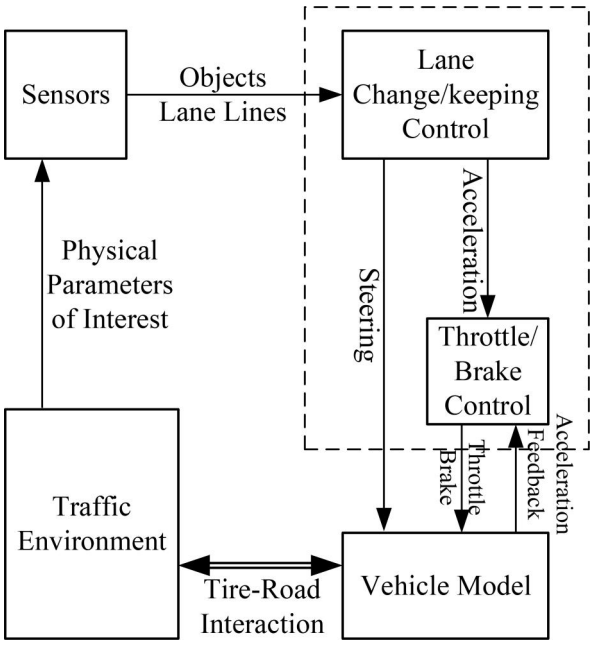

Figure 1. Automated driving system for lane change and lane keeping.

2.2. Traffic environment

This paper considers the control problems of automated vehicles running on the structured roads as shown in Figure 2, where the solid black lines and the dashed black lines represent the road boundaries and the lane markings, respectively. The icon of a sedan represents the ego vehicle that is an automated vehicle controlled by the proposed method, while the gray rectangles are the surrounding vehicles around the controlled one, regardless of whether they are automated or human-driven.

It is assumed that the lane markings, the road boundaries, and the surrounding vehicles or other objects within a certain range can be detected by the sensors mounted on the ego vehicle. More specifically, the perception system of the automated vehicle can provide a set of polynomials describing the lane markings and the road boundaries with respect to the coordinate system of the sensors. The reference trajectory $\boldsymbol{r}(t)$ in Equation (1a) consists of points related to those polynomials. Sensors can also detect the distance, detection angle, velocity, and heading angle of

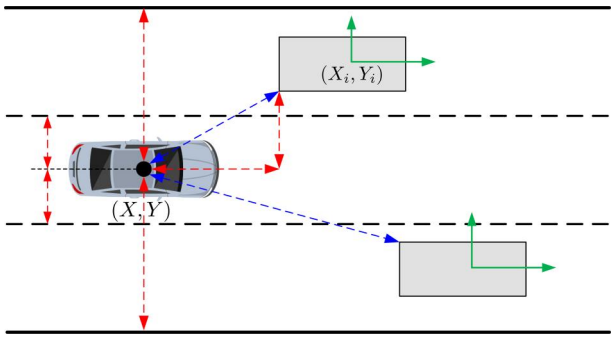

Figure 2. Traffic environment around the automated vehicle.

the surrounding objects. The world coordinate of the center of gravity (CG) of the ego vehicle is (X, Y), which can be precisely estimated by the on-board sensors such as GPS and IMUs.

2.3. Vehicle dynamic constraints

This subsection introduces a simple nonlinear 2-D vehicle dynamic model that formulates the dynamics constraints for the control problem of the ego vehicle. As shown in Figure 3, $X-Y$ is the world coordinate system, X_B-Y_B is the body-fixed coordinate system of the ego vehicle, CG is the center of gravity of the vehicle, point A and point B are the center of the front and rear tire, respectively. The differential equations describing the vehicle dynamics are written as follows.

$$m_0\dot{u}_x = m_0 a_x + m_0 u_y \gamma \tag{2}$$

$$m_0\dot{u}_y = F_{fy} + F_{ry} - m_0 u_x \gamma \tag{3}$$

$$I_z\dot{\gamma} = F_{fy} l_f - F_{ry} l_r \tag{4}$$

$$\dot{\psi} = \gamma \tag{5}$$

$$\dot{X} = u_x \cos\psi - u_y \sin\psi \tag{6}$$

$$\dot{Y} = u_x \sin\psi + u_y \cos\psi. \tag{7}$$

Herein, m_0 is the mass of the ego vehicle, l_f is the distance from point A to CG, l_r is the distance from point B to CG, I_z is the moment of inertia around the vertical axis through CG. u_x and u_y are the longitudinal and lateral velocities of the vehicle in the body-fixed coordinate system. ψ is the angle from the X-axis to the longitudinal axis of the vehicle body AB. γ is the yaw rate of the vehicle, $\gamma = \dot{\psi}$. (X, Y) is the world coordinate of CG, which is consistent with the ego vehicle in Figure 2. a_x is the longitudinal acceleration, which is treated as one of the control commands of the upper-layer control system.

In Equations (3)–(4), F_{fy} and F_{ry} are the total lateral forces of the front and rear tires, which can be

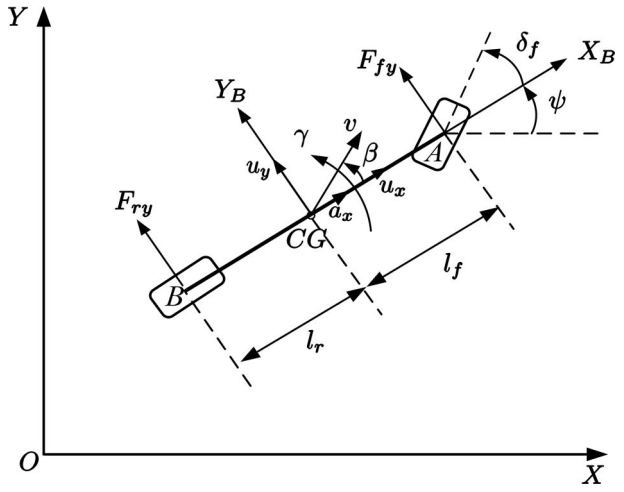

Figure 3. Vehicle dynamic model.

calculated by the following equations of tire dynamics (Rasekhipour et al., 2017).

$$F_{fy} = C_f\left(\delta_f - \frac{u_y + l_f\gamma}{u_x}\right), \tag{8}$$

$$F_{ry} = C_r\left(-\frac{u_y - l_r\gamma}{u_x}\right), \tag{9}$$

where C_f and C_r are the cornering stiffness coefficients of the front and rear tires, respectively. In Equations (2)–(9), u_x, u_y, γ, ψ, X, Y, δ_f and a_x are variables in the time domain, $\dot{u}_x$, $\dot{u}_y$, $\dot{\gamma}$, $\dot{\psi}$, $\dot{X}$ and $\dot{Y}$ are the time derivatives of u_x, u_y, γ, ψ, X and Y. The steering angle of the front tires δ_f is another control variable of the upper control module. Then, defining the state variable as $\boldsymbol{x} = [u_x, u_y, \gamma, \psi, X, Y]^{\mathrm{T}}$ and the control variable as $\boldsymbol{u} = [\delta_f, a_x]^{\mathrm{T}}$, the explicit form of f_0 in Equation (1b) can be obtained by combining Equations (1)–(9).

To make the problem more feasible and reduce the computation burden, the nonlinear dynamic system is linearized around its operating point. Assuming that the vehicle runs straight at a steady longitudinal speed of $u_x = u_0 > 0$, and u_y, γ and ψ are very small in magnitude at time t, the linearized system can be written as

$$\dot{\boldsymbol{x}} = \boldsymbol{A}(t)\boldsymbol{x} + \boldsymbol{B}(t)\boldsymbol{u}, \tag{10}$$

where

$$\boldsymbol{A}(t) = \begin{bmatrix} 0 & 0 & 0 & 0 & 0 & 0 \\ 0 & -\frac{C_f+C_r}{m_0 u_0} & \frac{-C_f l_f + C_r l_r}{m_0 u_0} - u_0 & 0 & 0 & 0 \\ 0 & \frac{-C_f l_f + C_r l_r}{I_z u_0} & -\frac{C_f l_f^2 + C_r l_r^2}{I_z u_0} & 0 & 0 & 0 \\ 0 & 0 & 1 & 0 & 0 & 0 \\ 1 & 0 & 0 & 0 & 0 & 0 \\ 0 & 1 & 0 & u_0 & 0 & 0 \end{bmatrix}, \tag{11}$$

$$\boldsymbol{B}(t) = \begin{bmatrix} 0 & 1 \\ \frac{C_f}{m_0} & 0 \\ \frac{C_f l_f}{I_z} & 0 \\ 0 & 0 \\ 0 & 0 \\ 0 & 0 \end{bmatrix}. \quad (12)$$

Then, discretizing the state space system by using the zero-order hold (ZOH), the discrete system that can be applied to the digital control system is obtained as

$$\boldsymbol{x}_{k+1} = \boldsymbol{A}_k \boldsymbol{x}_k + \boldsymbol{B}_k \boldsymbol{u}_k, \quad (13)$$

where $\boldsymbol{A}_k = e^{\boldsymbol{A}(t)\Delta t}$, $\boldsymbol{B}_k = \int_0^{\Delta t} e^{\boldsymbol{A}(t)\tilde{t}} \mathrm{d}\tilde{t} \boldsymbol{B}(t)$, and Δt is the sampling time of the control system.

2.4. Collision-avoidance constraints

This subsection describes the collision-avoidance constraints in Equation (1e). The signed distance function is a popular theoretical tool to detect collision for full-dimensional objects (X. Zhang et al., 2021). The signed distance function between the ego vehicle and the obstacle is defined as

$$sd(\mathcal{E}(\boldsymbol{x}), \mathcal{O}) := dist(\mathcal{E}(\boldsymbol{x}), \mathcal{O}) - pen(\mathcal{E}(\boldsymbol{x}), \mathcal{O}), \quad (14)$$

where $\mathcal{E}(\boldsymbol{x})$ is the convex set of points occupied by the ego vehicle, $\mathcal{O}$ is the convex set of points occupied by the full-dimensional objects in the traffic environment around the ego vehicle, $dist(\cdot,\cdot)$ and $pen(\cdot,\cdot)$ are the distance and penetration depth defined as

$$dist(\mathcal{E}(\boldsymbol{x}), \mathcal{O}) = \inf\{||T|| | (\mathcal{E}(\boldsymbol{x}) + T) \cap \mathcal{O} \neq \emptyset\}, \quad (15)$$

$$pen(\mathcal{E}(\boldsymbol{x}), \mathcal{O}) = \inf\{||T|| | (\mathcal{E}(\boldsymbol{x}) + T) \cap \mathcal{O} = \emptyset\}. \quad (16)$$

The distance between two sets, which is nonzero for non-intersecting sets, is defined as the smallest translation T that puts two shapes in contact. The penetration depth, which is nonzero for overlapping shapes, is defined analogously as the minimum translation T that takes two shapes out of contact. Roughly speaking, the signed distance in Equation (14) is positive if $\mathcal{E}(\boldsymbol{x})$ and $\mathcal{O}$ do not intersect, and negative if they overlap.

The ego vehicle is not colliding with an object if the signed distance between them is positive. At the beginning of every control cycle $t = 0$, the sensor system can detect the number of obstacles in the field of view (FOV) of the sensors mounted on the ego vehicle and their accurate information, such as range, azimuth, velocity, and heading angle. For the sake of simplicity, the velocity of the obstacle is assumed to be constant during the prediction horizon $[0, T_p]$, then the future states of the obstacles from $t = 0$ to $t = T_p$ are accessible at the beginning of the collision-avoidance motion planning. Therefore, the collision-avoidance constraints in Equation (1e) can be rewritten as

$$sd(\mathcal{E}(\boldsymbol{x}(t)), \mathcal{O}_i(t)) > 0, \forall i \in \mathcal{N}_o, t \in [0, T_p], \quad (17)$$

where $\mathcal{N}_o$ is the set consisting of all the indexes of the obstacles in the FOV of sensors.

However, it is tough to take the full-dimensional collision-avoidance constraints into consideration when solving the motion planning problem with the constraints of vehicle dynamics. To reduce the complicity of the optimization problem in Equation (1), we utilize a rough-plan-and-fine-check strategy that applies a dilated elliptical constraint (Li et al., 2022; Li et al., 2021) instead at the optimization stage and then applies the full-dimensional collision-avoidance constraints in Equation (17) to check whether the collision would happen or not. The elliptical constraint is written as

$$\frac{(X - X_i)^2}{P_i} + \frac{(Y - Y_i)^2}{Q_i} \geqslant 1, \quad (18)$$

where (X_i, Y_i) is the coordinate of the ith obstacle, P_i and Q_i are two positive real numbers depending on the size of the obstacle, and P_i is much larger than Q_i because the lateral velocity is generally much lower than the longitudinal velocity in normal driving scenarios. If a collision were detected at the checking stage, P_i and Q_i would be increased to dilate the elliptical obstacle (Liu et al., 2017).

3. Lane-changing and lane-keeping control

3.1. Motivations

This section proposes a control scheme that solves the lane-changing and lane-keeping problems in a unified fashion. In other words, the lane-changing process is treated the same as the lane keeping. Thus, the automated driving control on the structural road is only about the lane-keeping control, which will significantly simplify the control system of the automated vehicle designed for normal tasks on the structural road.

Generally, lane changing and lane keeping are two basic kinds of driving behaviors when people are driving on structural roads such as urban roads or highways. Other kinds of complex driving behaviors can be considered as a combination of these two basic ones. For instance, the process of overtaking is typically divided into lane changing, lane keeping, and

another lane changing back to the original lane in a sequential manner (Dixit et al., 2020; Graf et al., 2019; Ortega et al., 2020) as demonstrated in Figure 4.

Typically, the control problem of the flexible driving process is dealt with by decomposing the whole into simple individual maneuvers, which can be easily solved without considering the long-term process of continuous driving. However, this kind of strategy renders vague boundaries between different maneuvers and redundant modules in control systems. To consider further, lane changing and lane keeping are different in terms of concepts, but there are no differences between them in the view of computers. If these two kinds of control problems are solved in a unified way, the structure of the control strategy can be straightforward and the scale of the control system can be reduced.

In the remainder of this section, we first generate the reference points for trajectory planning, then formulate the unified control method for lane keeping and lane changing, finally introduce the feedback control of throttle and brake.

3.2. Generation of reference points

Lane marking detection, which is a part of the perception system, is a fundamental but crucial step for trajectory or motion planning in intelligent driving systems (Zhang et al., 2021). However, the information flow and the connection between the perception system and the control system have not been fully investigated. Most detection methods output the coordinates of several points or pixels of lane markings in the image coordinate system. Then, a series of curve fitting methods are used to fix the broken lane marking edges and refine the detection results.

In this paper, different lane lines are modeled with different groups of polynomials relative to the sensor in the fitting step. For each lane line detected in the FOV of the sensor, the fitting method attempts to fit the entire lane line with a set of polynomials for longitudinal and lateral coordinates at first. If the maximum fitting error is larger than the threshold, then the interval of the lane line for fitting in this attempt is shortened until the maximum error does not exceed the limit. Then the rest of the lane line will be fitted with the same approach and a sequence of polynomials can be obtained at last. From the right to the left in the view of the sensor, one of the lane lines including the road boundary lines is modeled as

$$\mathbb{L}_j = \{\{P_X^{(j1)}, P_Y^{(j1)}\}, \{P_X^{(j2)}, P_Y^{(j2)}\}, ..., \{P_X^{(jM)}, P_Y^{(jM)}\}\}, \tag{19}$$

where $\mathbb{L}_j$ is a group consisting of at least one set of polynomials, j is the index of the lane line, M is the index of the last set of fitting polynomials, P_X and P_Y are polynomials fitted for longitudinal and lateral coordinates formulated as

$$P_{xy}^{jm} = a_{xy}^{jm} l^3 + b_{xy}^{jm} l^2 + c_{xy}^{jm} l + d_{xy}^{jm}, \tag{20}$$

where $xy \in \{X, Y\}$, $l \in [0, L_m]$. L_m is the length of the interval, which needs to be determined by the fitting method, along with the coefficients a_{xy}^{jm}, b_{xy}^{jm}, c_{xy}^{jm} and d_{xy}^{jm}. Cubic or quadratic polynomials are commonly used to fit curves of structural highways or normal city roads except for the intersections, not to mention small segments of lane lines in this approach. For example, the road shape in highway scenarios is modeled by a third-degree polynomial (Zhang, 2023); Chapuis et al. (2002) utilized quadratic and cubic polynomials to fit the road lines about 80 meters instead of small segments; Wang et al. (2019) established the quadratic curve model for the curved lane-line in the far field of view.

Then, the key points of these detected lane markings are defined as the points sampled from the lane lines represented by a sequence of polynomials in the same group with arc length of the product of the target velocity of the self-vehicle v_t and the sampling time of the control system Δt. Note that one segment may stretch over a polynomial and its following one as shown in Figure 5, in which the black circle denotes the end of a curve and the beginning of its following one modeled by two sequent sets of

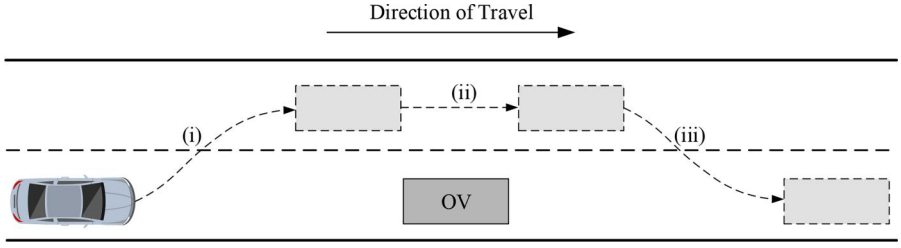

Figure 4. Generic schematic of an overtaking maneuver (i: lane change; ii: lane keeping; iii: lane change; OV: object vehicle).(Dixit et al., 2020).

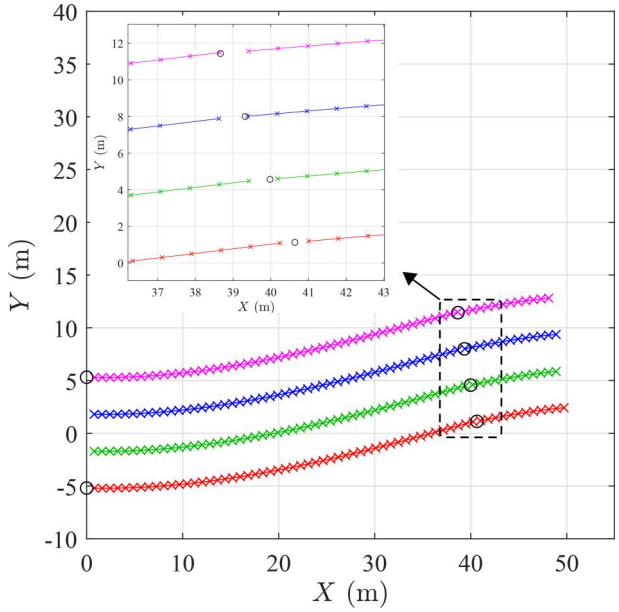

Figure 5. The cross marks denote the key points of lane lines and the black circle denotes the end of a curve and the beginning of its following one modeled by two sequent polynomials.

polynomials. The beginning points of segments, namely the key points, are represented by crosses in different colors for different lane lines.

Those key points with respect to the sensor system require to be transformed to the coordinates in the world coordinate system $X-Y$ by the following equation:

$$\begin{bmatrix} X \\ Y \end{bmatrix} = \begin{bmatrix} \cos\psi & -\sin\psi \\ \sin\psi & \cos\psi \end{bmatrix} \left(\begin{bmatrix} X_s \\ Y_s \end{bmatrix} + \begin{bmatrix} X_{\text{offset}} \\ Y_{\text{offset}} \end{bmatrix} \right), \tag{21}$$

where $[X_s, Y_s]^{\mathrm{T}}$ denotes the coordinate of the key point, and $[X_{\text{offset}}, Y_{\text{offset}}]^{\mathrm{T}}$ denotes the coordinate of the sensor in the world coordinate system. Then, the key points denoted by $\mathbb{P}_j$ can be obtained for each lane line with j representing the index of the lane line. Finally, the middle points composing the central line of each lane are the midpoints of the corresponding two key points on its right and left lane lines. The sequence of the middle points of the current lane in which the ego vehicle is driving is denoted by $\mathbb{P}_c$ and that of the target lane which the ego vehicle changes to is denoted by $\mathbb{P}_t$. As for the case of the lane keeping maneuver, $\mathbb{P}_t = \mathbb{P}_c$.

Three different ways are proposed in this paper to generate the reference points for the motion control of lane change and lane keeping. The first approach is to assign the middle points of the target lane within the prediction horizon directly to the reference points. In other words, the first reference generation method directly regards the middle points of the target lane as the reference points as shown in Figure 6(a), where the ego vehicle is changing to the left adjacent lane, the cross denotes the middle point of each lane, and the circle denotes the reference point.

The second approach is to attach the middle points of the target lane to the end of the reference points at the time of the beginning, and then roll the range of the reference points forward step by step. The number of total time steps of the prediction horizon in the discrete system is denoted by N_p ($N_p \in \mathbb{Z}^+$), $N_p = T_p/\Delta t$. Denote the middle points from the nearest to the farthest of the current lane within the prediction horizon by $(\mathbb{P}_c)_1^{N_p}$, then the reference points generated by this approach is written as

$$\boldsymbol{r}(k) = \{(\mathbb{P}_c)_1^{N_p-k-1}, (\mathbb{P}_t)_{N_p-k}^{N_p}\}, \tag{22}$$

where k is the prediction step, $k = 0, 1, \ldots, N_p - 1$, and $k = 0$ means the first control step when the lane change takes place. The second reference generation method forms the reference points from the middle points of the current lane and the target lane at the first N_p steps. Figure 6(b) presents an example of reference points generation for a lane change when $N_p - k = 5$, the reference points consist of $(N_p - k - 1)$ middle points of the current lane and $(k+1)$ middle points of the target lane. After N_p control steps from the beginning of the lane change, the reference points totally come from the middle points of the target lane.

The third reference generation method defines the reference point as one of the multi-section points that divide the line segment joining two corresponding middle points of the current lane and the target lane into N_p equal parts during the first N_p steps. The coordinates of the reference point can be calculated by using the internal section formula. To be precise, the sequence of the reference points is written as

$$\boldsymbol{r}(k) = \frac{N_p - k - 1}{N_p}(\mathbb{P}_c)_1^{N_p} + \frac{k+1}{N_p}(\mathbb{P}_t)_1^{N_p}, \tag{23}$$

with $k = 0, 1, \ldots, N_p - 1$. Obviously, after N_p control steps, all the reference points are sourced from the middle points of the target lane. Figure 6(c) illustrates a sequence of reference points among the middle points of two lanes generated by the third approach at the moment of k.

The three straightforward reference generation approaches proposed above are all quite easy to implement in practice. The first one would be selected if the time needed for the lane-changing maneuver has priority over other concerns in the control system of automated vehicles. The third one would be selected if the

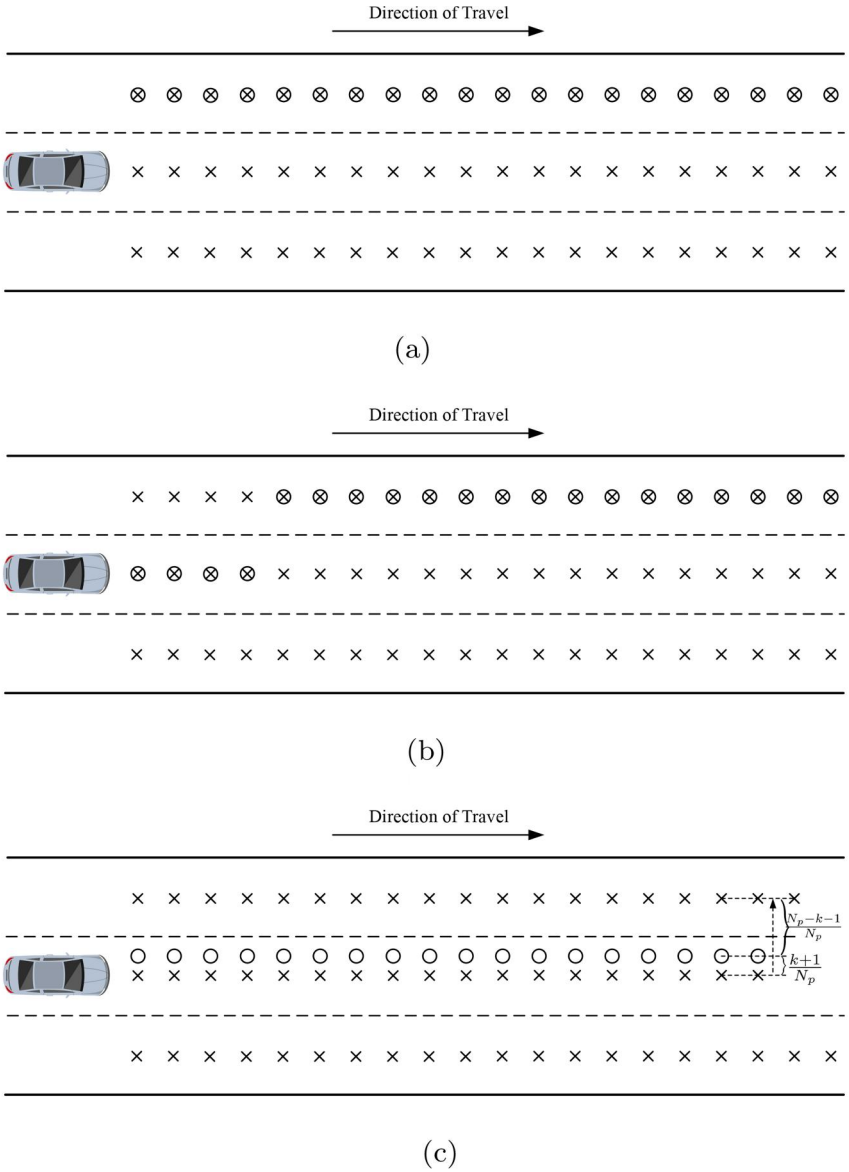

Figure 6. Generating the reference points for changing lanes to the left. The cross marker "×" denotes the Middle point of each lane, and the circle "○" denotes the reference point. (a) Reference points generated by the first approach. (b) Reference points generated by the second approach when $N_p - k = 5$. (c) reference points generated by the third approach at the moment of k, $k = 0, 1, \ldots, N_p - 1$.

small and steady steering is preferred. Otherwise, the second one would be selected. This paper provides choices for the system designer and the automated vehicles with these three reference generation approaches to meet different situations and requirements.

3.3. Formation of model predictive control

To isolate the tire dynamics and make the overall problem more tractable, the overall control problem is solved with an upper controller and a lower controller as previously presented in Figure 1. The upper controller is formulated within the framework of model predictive control to track the reference points and generate commands of acceleration and steering, while the lower one is utilizing the widely-used PID controller to implement the command of acceleration with actuators of the ego vehicle.

For the sake of the digital control, the model predictive control problem with the discrete dynamic system of the ego vehicle for lane-changing and lane-keeping maneuvers is formulated in the upper controller as follows:

$$\min_{\mathbf{U}} \sum_{n=0}^{N_p-1} J(\boldsymbol{x}_{n+1}, \boldsymbol{u}_n, \boldsymbol{r}_{n+1}) \tag{24a}$$

$$\text{s.t. } \boldsymbol{x}_{n+1} = \boldsymbol{A}_n \boldsymbol{x}_n + \boldsymbol{B}_n \boldsymbol{u}_n, n = 0, 1, \ldots, N_p - 1 \tag{24b}$$

$$\boldsymbol{x}_{\min} \preceq \boldsymbol{x}_n \preceq \boldsymbol{x}_{\max}, n = 1, 2, \ldots, N_p \tag{24c}$$

$$\boldsymbol{u}_{\min} \preceq \boldsymbol{u}_n \preceq \boldsymbol{u}_{\max}, n = 0, 1, \ldots, N_p - 1 \tag{24d}$$

$$\Delta\boldsymbol{u}_{\min} \preceq \boldsymbol{u}_n - \boldsymbol{u}_{n+1} \preceq \Delta\boldsymbol{u}_{\max}, n = 0, 1, \ldots, N_p - 2 \tag{24e}$$

$$\Delta\boldsymbol{u}_{\min} \preceq \boldsymbol{u}_{-1} - \boldsymbol{u}_0 \preceq \Delta\boldsymbol{u}_{\max} \tag{24f}$$

$$\frac{(X_n - X_{i,n})^2}{P_i} + \frac{(Y_n - Y_{i,n})^2}{Q_i} - 1 \geqslant 0, \quad n = 1, 2, \ldots, N_p, i = 1, 2, \ldots, N_o \tag{24g}$$

$$\boldsymbol{x}_0 = \boldsymbol{x}_k. \tag{24h}$$

In Equation (24a), $\mathbf{U} = [\boldsymbol{u}_0^{\mathrm{T}}, \boldsymbol{u}_1^{\mathrm{T}}, \ldots, \boldsymbol{u}_{N_p-1}^{\mathrm{T}}]^{\mathrm{T}}$ represents the sequence of the control commands that need to be solved. n is the prediction step, $n = 1, 2, \ldots, N_p - 1$. The objective function is written as

$$J(\boldsymbol{x}_{n+1}, \boldsymbol{u}_n, \boldsymbol{r}_{n+1}) = \boldsymbol{u}_n^{\mathrm{T}} S \boldsymbol{u}_n + q(v_t - \boldsymbol{C}_1 \boldsymbol{x}_{n+1})^2 + (\boldsymbol{r}_{n+1} - \boldsymbol{C}_2 \boldsymbol{x}_{n+1})^{\mathrm{T}} R (\boldsymbol{r}_{n+1} - \boldsymbol{C}_2 \boldsymbol{x}_{n+1}), \tag{25}$$

where S and R are semi-definite matrices, q is a constant coefficient, v_t is the target velocity mentioned in the previous subsection, the $\boldsymbol{C}_1$ and $\boldsymbol{C}_2$ are binary matrices that extract the longitudinal velocity and the coordinates of the ego vehicle from the full state variable, respectively. $\boldsymbol{r}_{n+1}$ represents the $(n+1)$-th element of the sequence of reference points $\boldsymbol{r}_k$. The first term of the right-hand side of Equation (25) represents the control cost, while the second term and the third term reflect the penalties on the tracking deviations of the target speed and the reference trajectory, respectively.

The equality constraints in Equation (24b) are the discrete system of the ego vehicle's dynamics derived from Equation (1b). Equations (24c)–(24d) are the basic limits of the state and control variables. Equation (24e) presents the constraints of the change between two adjacent control variables. An extra constraint is introduced in Equation (24f) for the first element of the control sequence based on the reason that the predictive control sequence should be closely related to the last executed control command denoted by $\boldsymbol{u}_{-1}$. Equation (24g) lists the collision-avoidance constraints that have been explained in Equation (18). $\boldsymbol{x}_0 = \boldsymbol{x}_k$ in Equation (24h) means that the initial condition of the control predictive problem is the current state of the ego vehicle at the system time step k.

By solving the predictive control problem in Equation (24) at each control step, the upper controller can generate a sequence of the control commands of steering and acceleration, the first acceleration of which will be delivered to the lower controller. It is straightforward to transform the predictive control problem to an optimization problem with constraints of the control sequence.

3.4. Feedback control of throttle and brake

To implement the acceleration command given by the upper controller, a feedback control scheme of throttle and brake is proposed as demonstrated in Figure 7, where a_x and a_x' are the acceleration command and the estimated acceleration respectively. If $a_x > a_x'$, a PID controller for the throttle control is activated. Otherwise, another PID controller for the brake control is in charge of the longitudinal acceleration. The control frequency of the acceleration is assumed to be f_a, which is a multiple of the frequency of the discrete system in Equation (13).

4. Simulations, results, and discussions

To study the performance of the proposed unified model predictive control method of automated vehicles for lane-keeping and lane-changing maneuvers, numerical simulations were conducted on the platform of PreScan, which is a software tool designed as a development environment for intelligent transportation systems and intelligent vehicle systems and supports a seamless interface with MATLAB and Simulink. This section reveals the details of the simulation as well as some results.

4.1. Simulation setup

A model of the Audi A8 Sedan offered by PreScan is chosen as the dynamic model of the ego vehicle in the simulation. The parameters of the vehicle dynamics appeared in Subsection 2.3 and their corresponding values which are extracted from the default dynamics configuration of this model in PreScan are listed in Table 1. The length of the prediction horizon T_p is 2 s, and the sampling time interval Δt is 0.05 s, then the total number of the sampling interval $N_p = 40$. Table 2 demonstrates some parameters related to the control method in Equation (24). In addition, the constraints of states $\boldsymbol{x}_{\min}$ and $\boldsymbol{x}_{\max}$ can be derived

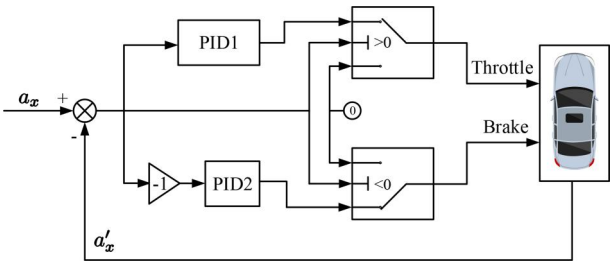

Figure 7. Feedback control of throttle and brake.

Table 1. Parameters of vehicle dynamics.

Parameter	Value (unit)	Parameter	Value (unit)
m_0	1820 (kg)	I_z	3746 (kg · m^2)
l_f	1.170 (m)	l_r	1.770 (m)
C_f	72653 (N/rad)	C_r	121449 (N/rad)

Table 2. Parameters of the control method.

Parameter	Value (unit)	Parameter	Value (unit)
Δt	0.05 (s)	T_p	2 (s)
$\boldsymbol{u}_{\min}$	$[-0.4363, -10]^{\mathrm{T}}$	$\boldsymbol{u}_{\max}$	$[0.4363, 3]^{\mathrm{T}}$
$\Delta\boldsymbol{u}_{\min}$	$[-0.1, -0.5]^{\mathrm{T}}$	$\Delta\boldsymbol{u}_{\max}$	$[0.1, 0.5]^{\mathrm{T}}$
P_i	8.0 (m)	Q_i	4.0 (m)
S	diag(1, 1)	R	diag(0.05, 0.05)
q	0.05	N_p	40

from the limitations in Equation (26) with other elements limited in a reasonably large domain instead of the whole infinite space for the consideration of the computational feasibility.

$$\begin{aligned} -1.5\ [\mathrm{rad/s}] \le \gamma \le 1.5\ [\mathrm{rad/s}], \\ -5.0\ [\mathrm{rad}] \le \psi \le 5.0\ [\mathrm{rad}]. \end{aligned} \tag{26}$$

Two virtual sensors are deployed on the ego vehicle in our simulation experiments, one is the lane marker sensor called ALMS and another one is the object sensor called AIR. The lane marker sensor is mounted on the roof of the ego vehicle at the point with coordinates (0.23, 0, 1.32)[m] in the ego vehicle's body-fixed coordinate system, while the object sensor is attached to the front bumper at the point with coordinates (2.17, 0, 0.37)[m] with respect to the *CG* of the ego vehicle.

A section of a structured road is constructed with straight road segments and bend road segments in the PreScan experiment editor. Some test scenarios are defined to evaluate the performance of the automated driving system implemented with the proposed unified predictive control for lane keeping and lane changing, which are two normal human-defined driving behaviors that form the whole process of every daily drive. Based on these two driving behaviors, several scenarios are constructed for testing as follows.

Scenario 1: The ego vehicle changes to the adjacent lane because of the slow preceding vehicle, then keeps in its current lane and maintains a steady speed.

Scenario 2: The ego vehicle keeps in its lane or changes lanes several times on a high-curvature road.

Scenario 3: The ego vehicle overtakes a slow preceding obstacle vehicle and deals with an emergency while changing lanes.

The above-mentioned scenarios are only some of the many cases that might occur when people are driving on a structured road. Nevertheless, they can evaluate the performance of the automated driving control system in observing obstacle avoidance and lateral and longitudinal maneuverability. The first scenario investigates the performance of lane changing if the current lane is occupied by other vehicles and the ability to keep driving in the current lane and follow the preceding vehicle. The second scenario studies the lane-keeping and lane-changing performance of the proposed control method on high-curvature road sections. The third scenario is employed to evaluate the comprehensive applicability of the proposed method in various lane-changing and lane-keeping situations.

4.2. Simulation results

4.2.1. Scenario 1

In this scenario, the ego vehicle maintains a steady speed of 16 [m/s] in the middle lane of the straight road at the beginning, while there is an obstacle vehicle moving ahead of the ego vehicle at a speed of 10 [m/s] in the same lane. The initial distance between the ego vehicle and the obstacle vehicle is larger than 60 meters. The path of the obstacle vehicle is configured with the centerline of its current lane. After capturing the obstacle vehicle in the FOV and realizing their distance is becoming smaller than the safe following distance, the ego vehicle chooses to make a lane change to the left to avoid the collision. Figure 8 presents some results of the lane changing process, the reference points of which are generated by the third method mentioned in Subsection 3.2. The trajectory of the lane changing is shown in Figure 8(a), which demonstrates that the ego vehicle accomplishes the lane-changing process smoothly. The steering control and the corresponding lateral acceleration of this process are presented in Figure 8(b). It is noted that the steering angle of the front tire is pretty small during this process, which means that subtle controls in steering are made for lane changing by the proposed method.

Three kinds of lane changing using reference points generated by different methods are compared and presented in Figure 9, where Figure 9(a) shows the trajectories of lane changing fulfilled by the proposed method and Figure 9(b) presents the steering controls. Results manifest that the ego vehicle is steered swiftly in response to the lane change by using the first reference generation approach. The maximum steering angle is very large and the whole process is completed in a very short time. This approach is very similar to the lane-changing behavior of aggressive driving or in

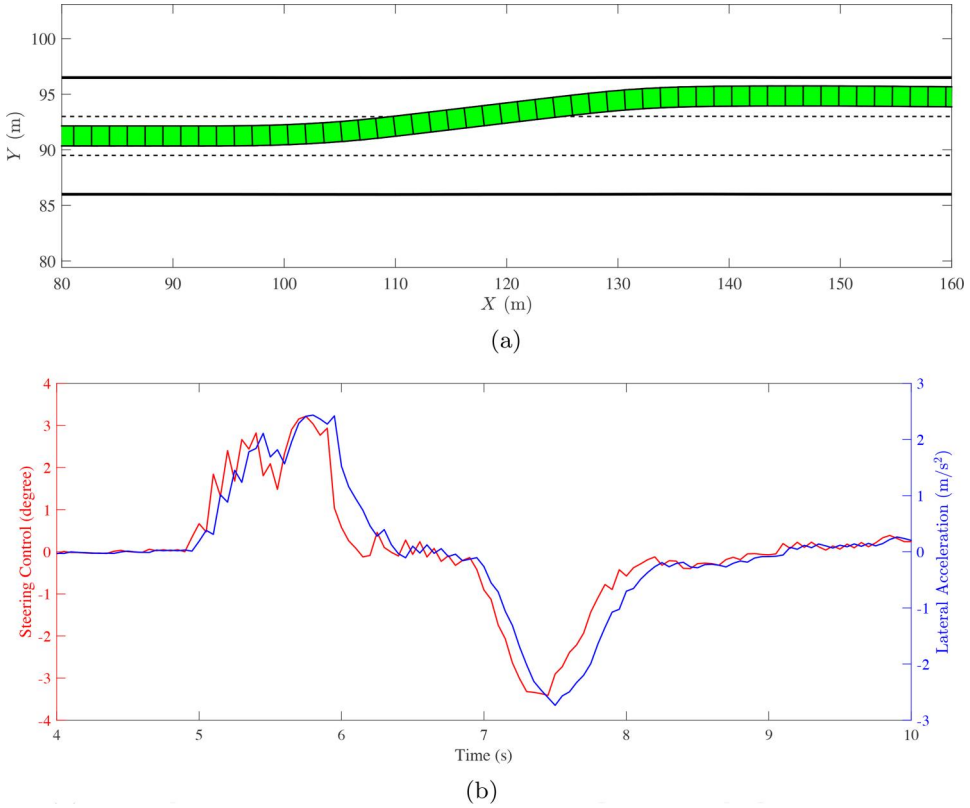

Figure 8. A lane change in scenario 1. (a) Lane-changing trajectory of the ego vehicle. (b) Steering control and lateral acceleration during lane changing.

an emergent situation. The second reference generation approach reacts to the lane changing most slowly, but the amplitude of the steering angle is not the smallest. By using the reference points generated by the third approach, the proposed method starts to steer the ego vehicle immediately with moderate steering angles. It turns out that the trajectory of the ego vehicle using this approach is the smoothest among these three. The duration of the steering for the lane change in this case is about 3.10 s, which is much larger than the lane-changing time (1.50 s) if the first reference generation method is deployed. Its performance of the lane-changing control is comparable to the normal driving behavior of a conservative human driver who tends to steer slower with small angles (Yang et al., 2021; Chen & Wang, 2018; Li et al., 2019).

Afterward, the ego vehicle moves in the rightmost lane on the straight road with a curved road ahead at a speed of 16 [m/s]. There is an obstacle vehicle running ahead in the same lane at a nominal speed of 16 [m/s] with a slight fluctuation. The path of the obstacle vehicle is inherited from the centerline of the rightmost lane and the speed profile is set with the smooth acceleration and deceleration of 0.3 [m/s^2] in the SpeedProfile Editor of PreScan. The initial distance between these two vehicles is around 60 meters. The simulation results of this scenario are shown in Figure 10. Figure 10(a) presents the trajectory of the ego vehicle on the curved road. The green rectangles demonstrate the position and orientation of the ego vehicle sampled from the full trajectory of the control process. As presented in Figure 10(b), the steering control commands are generated by the proposed control method to keep the ego vehicle in its current lane and prevent it from running outside of the road boundaries during the curve driving. Figure 10(b) also shows that the lateral acceleration closely comes after the steering control command.

4.2.2. Scenario 2

Further experiments have been conducted under more complex road conditions to study the lane-keeping and lane-changing performance of the proposed control method on high-curvature road sections. In this case, the ego vehicle enters a high-curvature zigzag road composed of four pieces of curves whose radii are all equal to 40 meters. The target speed of the ego vehicle is 10 [m/s] while it is running on this road. The configuration of the road and the trajectory and the motions of the ego vehicle while keeping in the middle lane are displayed in Figure 11, where the dash-dot blue lines with filled circles attached to their

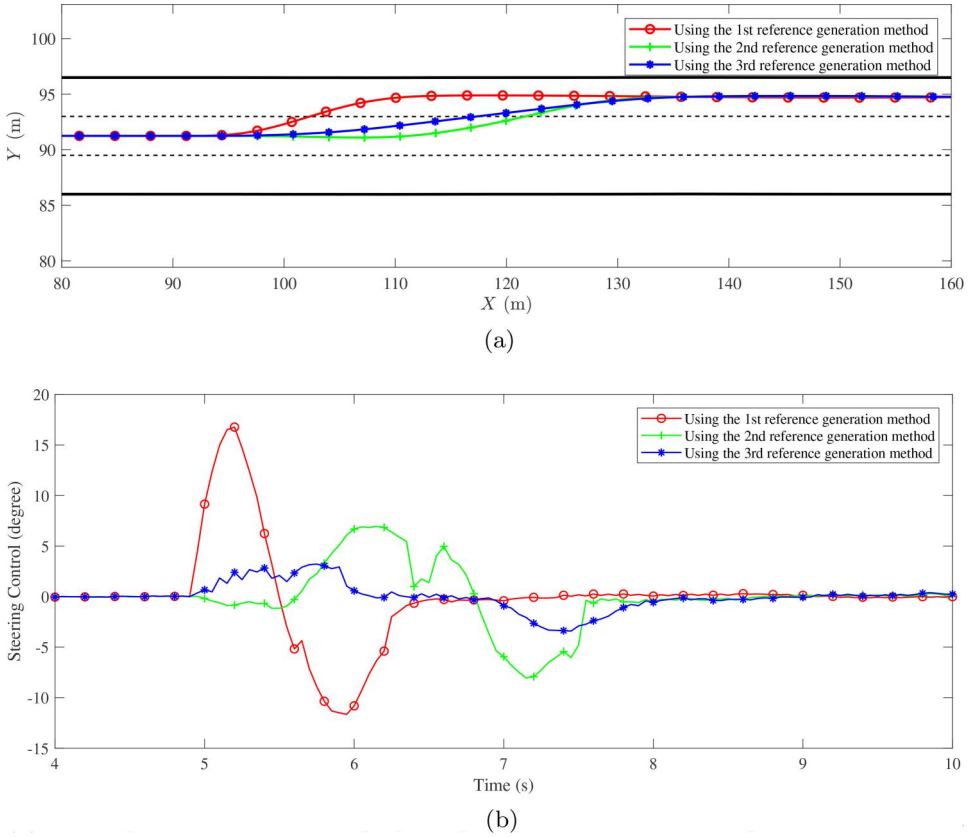

Figure 9. Comparisons between lane changes using three different reference generation methods. (a) Trajectories of lane changing. (b) Steering control of lane changing.

ends represent the radius of the curved road, the rectangle with solid green lines represents the ego vehicle, the solid red line is the trajectory of the ego vehicle. Meanwhile, the tracking error between the ego vehicle and the reference, which is the centerline of the middle lane during lane keeping, is presented in Figure 12. The maximum and average tracking errors are 0.791 [m] and 0.326 [m], respectively, which indicate that the ego vehicle's body remains in the lane while keeping lanes on this high-curvature road.

Applying the third reference generation method described in Section 3.2, the trajectory and the motions of the ego vehicle when it changes lanes four times on this zigzag road in a short period of about 35 s are presented in Figure 13, where the rectangle with dash-dot blue lines denotes the pose of the ego vehicle while changing lanes. Except for trajectories of lane changes, the maximum and average tracking errors between the ego vehicle and the centerlines of the lane where it is are 0.939 [m] and 0.398 [m], respectively, which are comparable to the case of lane keeping in the middle lane. Each lane change in this scenario lasts for about 3 s.

Moreover, experiments with lane changes using another two reference generation methods have also been conducted on the high-curvature road. The trajectories of the ego vehicle are presented in Figure 14, where the solid red line, the dashed green line, and the dash-dot blue line denote the trajectories accomplished by using the first, the second, and the third reference generation method, respectively. Figure 14 only displays two-thirds of the whole driving process to make the comparison of three reference generation methods more visible. As demonstrated in *Scenario 1*, the first reference generation method guides very swift lane changes, the second one reacts to the lane change slowly, while the third one leads moderate lane-changing maneuvers.

To evaluate the tracking performance of the proposed controller when the ego vehicle keeps in its lane or changes lanes on a high-curvature road, key performance indicators, such as the average, the maximum, and the root mean square value of the tracking error, are calculated and summarized in Table 3. The tracking performance indicators of the lane keeping are calculated based on the entire process of driving in the center lane on this high-curvature road, while the tracking performance indicators of the ego vehicle when it changes lanes multiple times are based on the segments of trajectories excluding the lane-changing parts due to the lack of comparability among controllers concerning

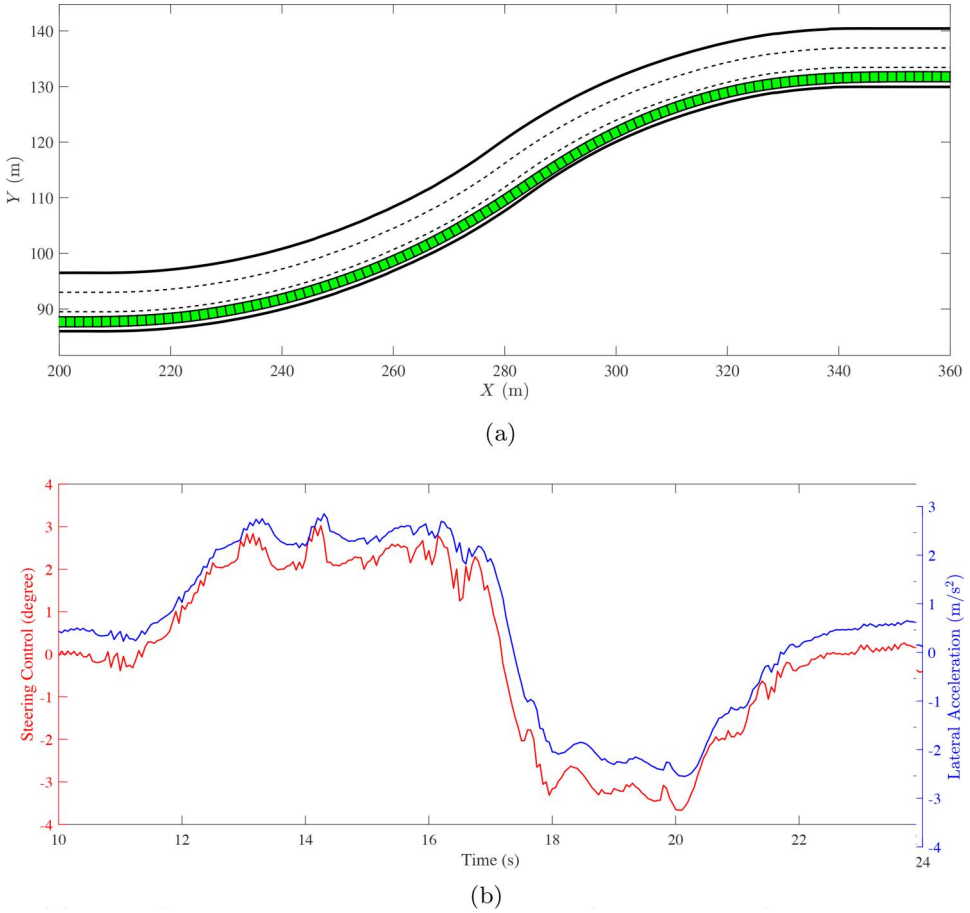

Figure 10. Lane keeping in scenario 1. (a) Trajectory of the ego vehicle on the curved road. (b) Steering control and lateral acceleration during a curve driving.

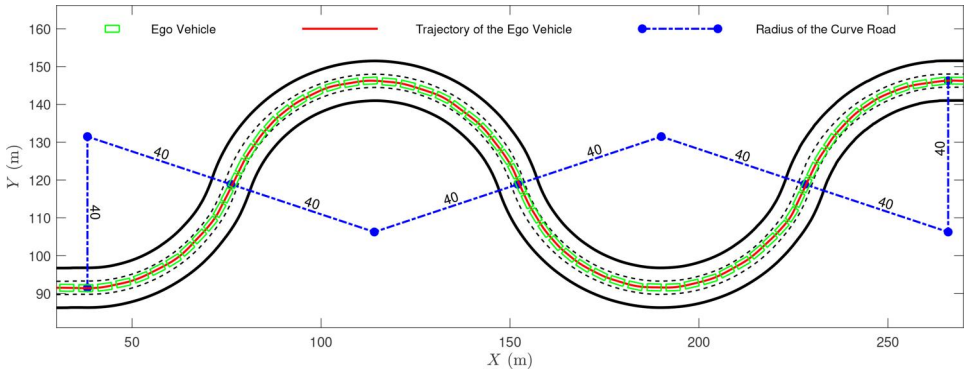

Figure 11. Lane keeping on a high-curvature road. (The rectangle with solid green lines represents the ego vehicle. The solid red line is the trajectory of the ego vehicle. The dash-dot blue lines with filled circles attached to their ends represent the radius of the curved road.).

their different and time-variant references. Considering the width of each lane is 3.5 [m] and the width of the ego vehicle is 1.8 [m], results show that the proposed control method keeps the body of the ego vehicle in the target lane most of the time in lane-keeping and lane-changing scenarios on the high-curvature road. The performance of the proposed control method in our paper is acceptable according to the key performance indicators in Table 3 compared to the state-of-the-art literature (Cheng et al., 2021; Hu & Zhao, 2021; Stano et al., 2023; Wang et al., 2021) focusing on the path tracking method based on Model Predictive Control.

4.2.3. Scenario 3

In this scenario, the ego vehicle realizes an overtaking maneuver and deals with an emergency while

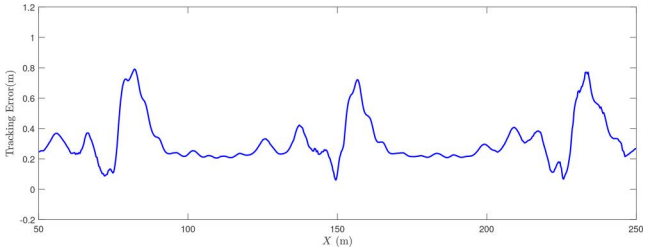

Figure 12. The tracking error between the ego vehicle and the lane centerline.

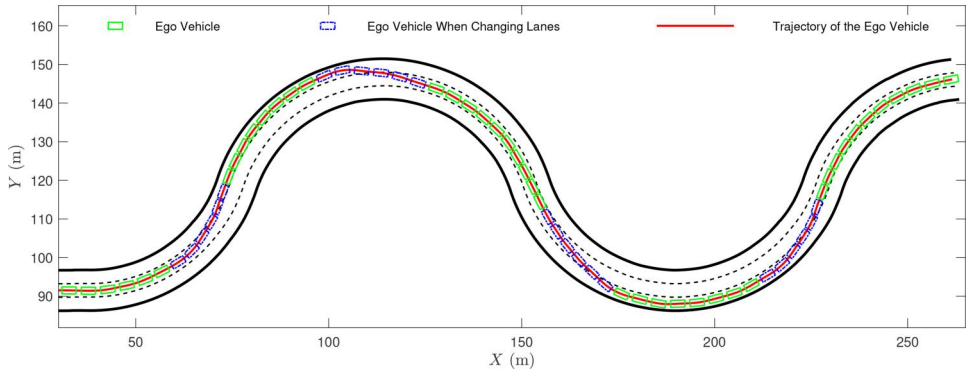

Figure 13. Lane changes on a high-curvature road. (The rectangle with dash-dot blue lines represents the ego vehicle while changing lanes. The rectangle with solid green lines represents the ego vehicle while keeping lanes. The solid red line is the trajectory of the ego vehicle.).

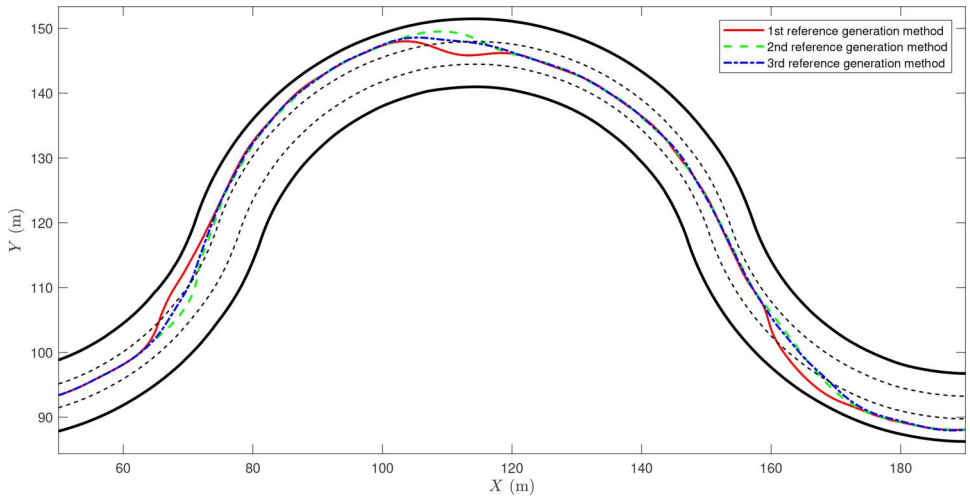

Figure 14. Trajectories of the ego vehicle when it changes lanes on a high-curvature road. (The solid red line, the dashed green line, and the dash-dot blue line denote the trajectories accomplished by using the first, the second, and the third reference generation method, respectively.).

changing lanes. The distance between the ego vehicle and a proceeding obstacle vehicle is 55 meters at the beginning of the simulation. There is another obstacle vehicle that is out of the FOV of the ego vehicle moving in the left adjacent lane. The initial speed of the ego vehicle is set to be 16 [m/s], and those two obstacle vehicles remain at the same constant speed of 10 [m/s]. There is a platoon of obstacle vehicles continuously moving at a speed of 15 [m/s] in the right adjacent lane.

After driving in its current lane for several seconds, the ego vehicle changes to the left lane to avoid colliding with the moving obstacle vehicle ahead before the gap becomes too small. The reference path of the MPC problem in Equation (24) is generated by the third approach for this lane-changing process. Then the ego vehicle keeps in the left lane temporarily. When passing by the first obstacle vehicle, the second one comes into the FOV of the ego vehicle. For the same reason as the first lane change, the ego vehicle should be able to

change back to the middle lane and at the same time it should be following the regulations of collision avoidance with two obstacles. This lane change should be finished swiftly, so the first reference generation approach is applied to guide the ego vehicle this time. The simulation results are shown in Figure 15, where Figure 15(a) presents the trajectory of the entire overtaking process of the ego vehicle implemented by the proposed method, and Figure 15(b) depicts the steering angle generated by the upper control module and the lateral acceleration in response to the control.

An emergency occurs if the obstacle vehicle in the left adjacent lane is behind the ego vehicle and moves at a speed of 15 [m/s] at the beginning and increases to 18 [m/s] afterward. The ego vehicle keeps moving at a steady speed of 16 [m/s] in the middle lane, while there is an obstacle vehicle moving ahead of the ego vehicle at a speed of 10 [m/s] in the same lane. After capturing the preceding vehicle in the FOV and realizing their distance is becoming smaller and smaller, the ego vehicle chooses to change to the left lane instead of decreasing the speed to keep a safe distance. However, one second after the start of the lane change, the gap between the obstacle vehicle in the left lane and the ego vehicle becomes insufficient because of the acceleration of the obstacle vehicle.

There is no feasible solution for the ego vehicle to continue the lane-changing maneuver for collision avoidance. Therefore, the index of the original lane is assigned to the target lane in the proposed method. Without altering anything else of the controller, the ego vehicle automatically changes to the right lane and decreases the speed to keep a safe distance from the preceding obstacle vehicle in the middle lane. The trajectories of these vehicles are shown in Figure 16, where the rectangles with solid green lines represent the ego vehicle, the rectangles with dashed red lines represent the obstacle vehicle that is behind the ego vehicle at the beginning, rectangles with dots represent the platoon of the obstacle vehicles in the rightmost lane. The time when those vehicles pass by those positions is stamped inside those rectangles. The process of attempting a lane change and a change back to the original lane lasts for about four seconds in this scenario.

Table 3. Key performance indicators.

		Lane changes		
	Lane keeping	First reference generation method	Second reference generation method	Third reference generation method
Average [m]	0.326	0.361	0.451	0.398
RMS [m]	0.365	0.406	0.523	0.454
Maximum [m]	0.791	0.874	1.20	0.939

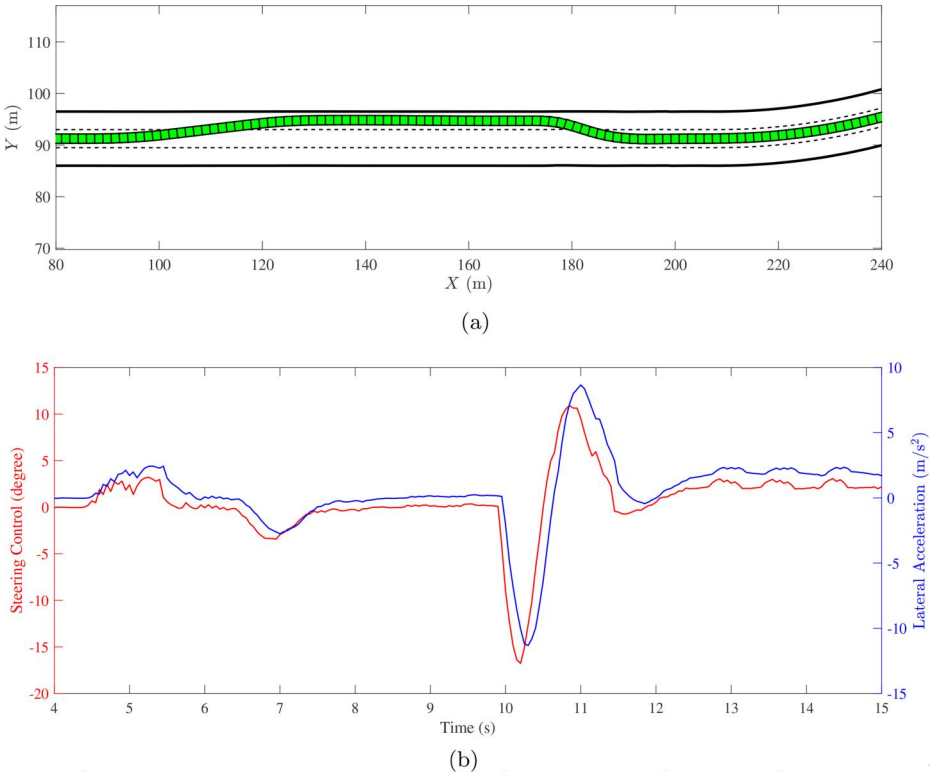

Figure 15. Overtaking in scenario 3. (a) Trajectory of the ego vehicle during overtaking. (b) Steering control and lateral acceleration of the ego vehicle during overtaking.

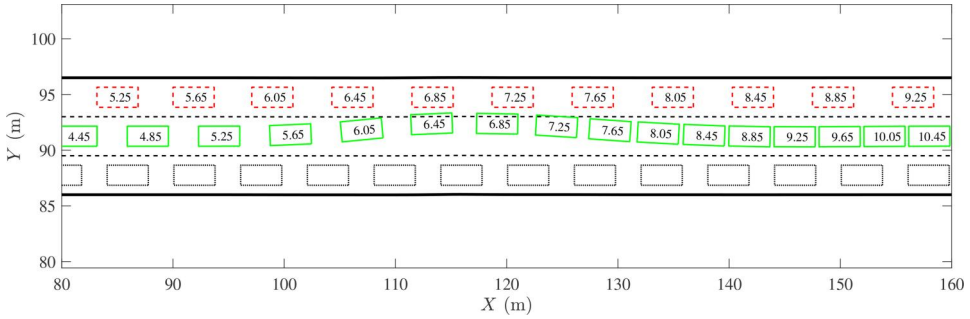

Figure 16. The ego vehicle changes back to its original lane because the traffic gap in the target lane is becoming insufficient. (The rectangle with solid green lines represents the ego vehicle. The number inside the rectangle represents the time.).

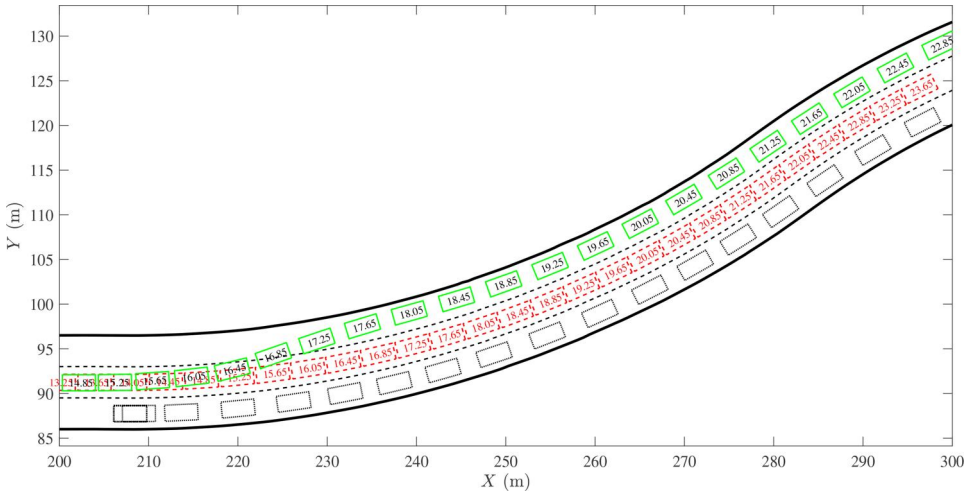

Figure 17. The ego vehicle changes again to the left adjacent lane on the curved road. (The rectangle with green solid lines represents the ego vehicle. The number inside the rectangle represents the time.).

Keeping in the middle lane and following the slower preceding vehicle, the ego vehicle gets a second chance to change lanes to the left after the approaching vehicle from behind passes by. Specifically, the ego vehicle is moving on a curved road at the speed of 10 [m/s] with a preceding vehicle at this time. When the decision of a lane change is made, the index of the left lane is assigned to the target lane and the target speed can be increased to a higher one in the proposed controller. The trajectories of these two vehicles are shown in Figure 17, where the rectangles with solid green lines represent the ego vehicle, and the rectangles with dashed red lines represent the preceding vehicle. Figures 16 and 17 show that the proposed control method has the capability to deal with emergencies in different situations no matter what the shape of the road is.

Compared to state-of-the-art methods, our method regards the lane-changing maneuver and the lane-keeping maneuver as the same. The reference generation is a transition period for the ego vehicle when it changes from one lane to another. This period can be tuned in simple manners to match any longer duration of the lane change when the decision is made as long as it is within the safety gap and accords with the vehicle dynamics. The simulation results of different scenarios demonstrate the comprehensive applicability of the proposed method in various lane-changing and lane-keeping situations.

There is no difference in the proposed control method for lane-keeping and lane-changing maneuvers, no matter whether on the straight road or the curved road. The results of these scenarios demonstrate the capabilities of our proposed method in various complex driving conditions.

4.3. Perception errors

Experiments have been conducted to investigate the impact of the perception errors on the final control accuracy of the automated vehicle for lane keeping on the curved road. In this case, the automated vehicle is driving steadily at the speed of 16 [m/s] when entering the S-shaped curve. If the perception errors exist,

Table 4. Average displacement errors of trajectory tracking.

	Proposed method without perception errors	Proposed method with perception errors ($T_{\text{Error}} = 1$)	Proposed method with perception errors ($T_{\text{Error}} = 2$)	Open-loop control with perception errors
ADE (m)	0.6710	0.6987	0.8123	1.2255

there would be longitudinal and lateral displacements of the reference for the trajectory tracking in the world coordinate system. It is assumed that the longitudinal and lateral displacements are both $\frac{\sqrt{2}}{2}$ [m], and the malfunction of the perception starts when the automated vehicle enters the curve road and lasts for T_{Error} seconds.

In the first experiment, the automated vehicle is controlled by the proposed method involving the perception system in the control loop and there are no perception errors. The second and the third experiments are similar to the first one except there are perception errors lasting 1 s and 2 s, respectively. In the last experiment, the perception system is not involved in the closed control loop, which means the proposed method is decoupled to an open-loop control and the perception errors that occurred at the beginning keep existing in the whole process.

The average displacement errors (ADEs) between the reference of the lane and the trajectories of the automated vehicle in those above experiments are presented in Table 4, which demonstrates that the perception errors decrease the accuracy of trajectory tracking. Furthermore, compared to the open-loop control fashion, the proposed method involving the perception in the control loop greatly diminishes the impact of the perception errors on the control of the trajectory tracking. Figure 18 distinctly presents the ground-truth reference and the trajectories of the automated vehicle controlled by the proposed method without perception errors, the proposed method with perception errors ($T_{\text{Error}} = 2$), and the open-loop control with perception errors.

In this case, the target lane is the current lane, the three reference generation methods are equivalent to the control of lane keeping. At the same time, the ground-truth reference of lane keeping is the centerline of the lane. Therefore, these three reference generation methods would yield the same ADE under the same perception errors.

4.4. Comparative studies

This paper provides comparative studies of the proposed method and state-of-the-art works (Luo et al., 2016) and (Li et al., 2022) on driving comfort and efficiency instead of the tracking performance of the lane change control to validate the advantages of our method.

It is noted that there is no ground-truth trajectory for the automatic lane change in either state-of-the-art works or the proposed method in our paper. The planning of trajectories for lane-changing maneuvers is designed to meet their requirements with different objectives in state-of-the-art works, which is a top-down approach. In our paper, the reference generation is a transition period for the ego vehicle when it changes from one lane to another. The trajectory of the lane-changing maneuver is fulfilled optimally in a receding horizon with constraints of vehicle dynamics and obstacle avoidance, which is a bottom-up approach on the contrary. Thus, it may be misleading to compare the ADEs of our method with state-of-the-art works when the reference trajectories are not the same.

On the other hand, driving comfort and efficiency are important indicators to measure the performance of the automated vehicle. Calculations of driving comfort and efficiency can remain consistent among different lane-changing control methods. Therefore, comparative studies of the proposed method and two previous researches (Luo et al., 2016) and (Li et al., 2022) on these two indicators of automatic lane-change control have been conducted to evaluate the advantages of the proposed one over state-of-the-art methods. Besides, other performance parameters, such as the maximum longitudinal acceleration and the maximum lateral acceleration, are also compared with the method in Luo et al. (2016).

The cost function of the automated vehicle at the given trajectory is provided as follows.

$$\text{Cost}_{AV} = w_{AV}^{\text{comfort}} \cdot C_{AV}^{\text{comfort}} + w_{AV}^{\text{efficiency}} \cdot C_{AV}^{\text{efficiency}}, \tag{27}$$

where w_{AV}^{comfort} and $w_{AV}^{\text{efficiency}}$ are the weight coefficient of the comfort and efficiency, C_{AV}^{comfort} and $C_{AV}^{\text{efficiency}}$ are the cost of comfort and efficiency.

$$C_{AV}^{\text{comfort}} = \frac{\int_{t_s}^{t_e} |j_{AV,x}(t)|dt + \int_{t_s}^{t_e} |j_{AV,y}(t)|dt}{N_{AV}^{\text{comfort}}}, \tag{28}$$

$$C_{AV}^{\text{efficiency}} = \frac{\int_{t_s}^{t_e} |v_{AV}(t) - v_{\text{target}}|dt}{N_{AV}^{\text{efficiency}}}, \tag{29}$$

where $j_{AV,x}(t)$ and $j_{AV,y}(t)$ are the longitudinal and lateral jerk, which are the two most important factors

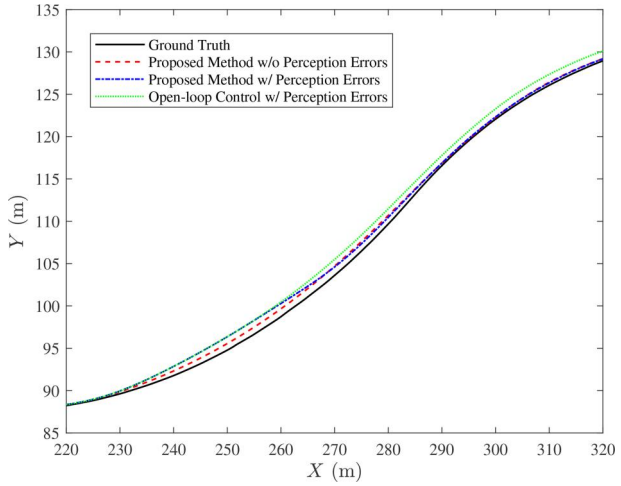

Figure 18. The ground-truth reference and the trajectories of the automated vehicle in different conditions.

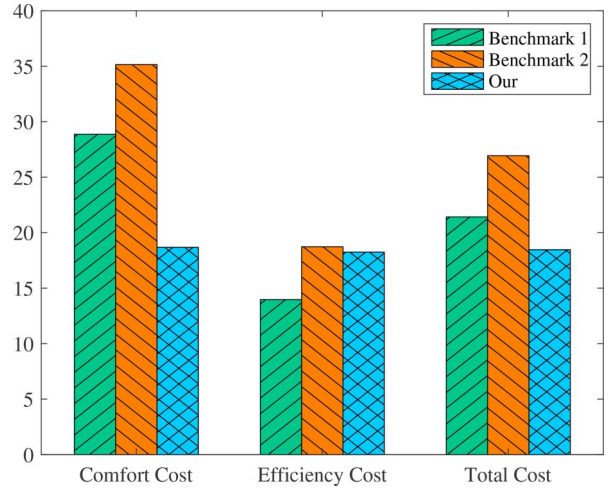

Figure 19. Comparison of the costs between the benchmark methods and our method.

Table 5. Costs of the lane change of the automated vehicle.

Cost of lane change	Benchmark method 1	Benchmark method 2	Our method
Cost of comfort	28.87	35.15	18.67
Cost of efficiency	13.97	18.73	18.25
Total cost	21.42	26.94	18.46

affecting the ride comfort. N_{AV}^{comfort} and $N_{AV}^{\text{efficiency}}$ are the normalized values of the corresponding terms to make the units consistent. t_s and t_e are the moments when the automated vehicle starts and ends the lane-changing maneuver. v_{target} is the target speed of the automated vehicle.

In this case, the automated vehicle is moving at a steady speed of 25 [m/s] in the middle lane of a straight road from the beginning, and starts to change to the adjacent lane in 5 s. The target speed of the AV is also 25 [m/s]. The cost of comfort and the cost of efficiency of the lane-changing maneuver of the automated vehicle are compared to the results of benchmark methods. Methods proposed in Luo et al. (2016) and (Li et al., 2022) are considered as the benchmark method 1 and the benchmark method 2, respectively. Table 5 lists the results of those three methods. The comparison of the bar charts displayed in Figure 19 demonstrates the advantages of our proposed method.

Furthermore, Table 6 shows some performance parameters of the lane-changing maneuver of the proposed method compared with the benchmark method in Luo et al. (2016) when the automated vehicle drives on the straight road at a speed of 100 [km/h] and changes to the adjacent lane once along the way. Here, $a_{x,\max}$ and $a_{y,\max}$ are the maximum longitudinal acceleration and the maximum lateral acceleration with respect to the body-fixed coordinate system of the automated vehicle. These parameters show that the proposed method guarantees a more comfortable lane change maneuver.

Table 6. Performance parameters (speed = 100 km/h).

	$\lvert a_{x,\max}\rvert (m/s^2)$	$\lvert a_{y,\max}\rvert (m/s^2)$
Benchmark method 1	3.48	1.81
Our method	0.1906	0.9298

4.5. Computation time

All the simulations presented in this work were carried out on an entry-level desktop computer with an Intel i5-12400F 2.50 GHz CPU, 16GB of RAM and an NVIDIA RTX 3060 GPU. The computation times of the proposed controller executed in every cycle in different scenarios described in Subsection 4.2 are plotted in Figure 20, which illustrates that most of the computation times are less than the control cycle, 0.05 s. Since industrial automated vehicles may have more computational power, our proposed method could satisfy the real-time control requirements.

4.6. Discussions

Compared to the scenarios simulated in this section, which are straightforward and monotonous, driving maneuvers in real life are much more complex and flexible. Nevertheless, complicated driving processes on structural roads can be accomplished by elementary moves, namely, lane keeps and lane changes. Simulations of simple scenarios are utilized to illustrate the idea that lane change can be treated as lane keep and validate that the proposed method has the capability to fulfill lane-changing and lane-keeping maneuvers continuously.

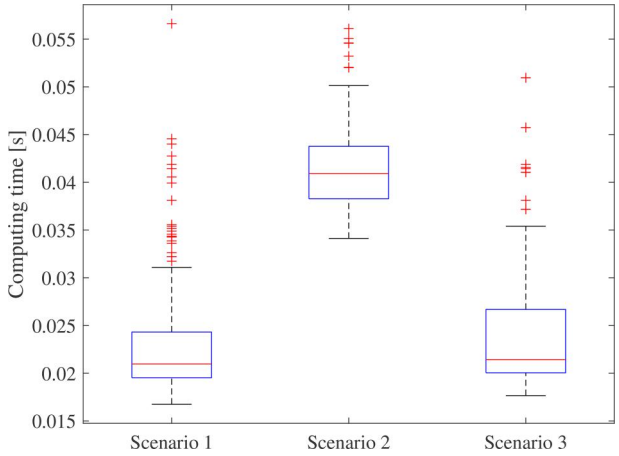

Figure 20. Computation times in different scenarios.

Simulations with computer tools are ideal, while the real-world traffic environment is full of uncertainties and risks. Nevertheless, simulations are powerful and necessary because they make it easier for us to validate our ideas without using expensive equipment and risking our safety. The perception of the traffic environment is one of the most important parts of the automated driving system, but it is not the focus of this study. Thanks to simulation platforms for offering handy tools to obtain the precise information of the road and the traffic, so that we can easily control the vehicle in a closed-form.

Readers who are interested in our work can watch the videos captured during simulations on our website.[1]

5. Conclusions

This work designs the motion control of automated vehicles for combined lane keeping and lane changing. To make the driving process smoother and the control system simpler, lane changing is considered as another form of lane keeping. A unified model predictive control is proposed to formulate the control law of the ego vehicle in fulfilling lane-keeping and lane-changing maneuvers safely. The controller design forms a closed loop that consists of the perception of the road and the motion control of the ego vehicle by generating reference points from the lines detected. The proposed control framework is composed of a model predictive control in the upper module and a PID control in the lower module, which eliminates the complexity of the tire dynamics. Various driving scenarios are designed and simulated on the PreScan-MATLAB/Simulink joint simulation platform. The simulation results have verified the comprehensive capabilities of the proposed method in dealing with different driving behaviors including lane keeping and lane changing. Our future work will implement the proposed method on small-scale automated vehicles that allow fully self-contained testing of various motion control methods in field experiments.

Note

1. https://liujwei.github.io/research.html.

Disclosure statement

No potential conflict of interest was reported by the author(s).

ORCID

Wei Liu http://orcid.org/0000-0002-8662-7888
Yongqi Dong http://orcid.org/0000-0003-1159-9584

References

Arrigoni, S., Braghin, F., & Cheli, F. (2022). MPC trajectory planner for autonomous driving solved by genetic algorithm technique. *Vehicle System Dynamics*, 60(12), 4118–4143.

Chapuis, R., Aufrere, R., & Chausse, F. (2002). Accurate road following and reconstruction by computer vision. *IEEE Transactions on Intelligent Transportation Systems*, *3*(4), 261–270. https://doi.org/10.1109/TITS.2002.804751

Chen, Y., Wang, J. (2018). Personalized vehicle path following based on robust gain-scheduling control in lane-changing and left-turning maneuvers. *2018 Annual American Control Conference (Acc)* (pp. 4784–4789).

Chen, Z., Huang, X. (2017). End-to-end learning for lane keeping of self-driving cars. *2017 IEEE Intelligent Vehicles Symposium (iv)* (pp. 1856–1860).

Cheng, S., Li, L., Chen, X., Wu, J., & Wang, H-d,. (2021). Model-predictive-control-based path tracking controller of autonomous vehicle considering parametric uncertainties and velocity-varying. *IEEE Transactions on Industrial Electronics*, *68*(9), 8698–8707. https://doi.org/10.1109/TIE.2020.3009585

Cui, Q., Ding, R., Wei, C., & Zhou, B. (2021). Path-tracking and lateral stabilisation for autonomous vehicles by using the steering angle envelope. *Vehicle System Dynamics*, *59*(11), 1672–1696. https://doi.org/10.1080/00423114.2020.1776344

Dixit, S., Montanaro, U., Dianati, M., Oxtoby, D., Mizutani, T., Mouzakitis, A., & Fallah, S. (2020). Trajectory planning for autonomous high-speed overtaking in structured environments using robust MPC. *IEEE Transactions on Intelligent Transportation Systems*, *21*(6), 2310–2323. https://doi.org/10.1109/TITS.2019.2916354

Do, Q. H., Tehrani, H., Mita, S., Egawa, M., Muto, K., & Yoneda, K. (2017). Human drivers based active-passive model for automated lane change. *IEEE Intelligent Transportation Systems Magazine*, *9*(1), 42–56. https://doi.org/10.1109/MITS.2016.2613913

Falcone, P., Borrelli, F., Asgari, J., Tseng, H. E., & Hrovat, D. (2007). Predictive active steering control for

autonomous vehicle systems. *IEEE Transactions on Control Systems Technology*, *15*(3), 566–580. https://doi.org/10.1109/TCST.2007.894653

Fu, Y., Li, C., Yu, F. R., Luan, T. H., & Zhang, Y. (2021). *A survey of driving safety with sensing, vehicular communications, and artificial intelligence-based collision avoidance* [Paper presentation]. IEEE Transactions on Intelligent Transportation Systems.

Gao, Y., Gray, A., Tseng, H. E., & Borrelli, F. (2014). A tube-based robust nonlinear predictive control approach to semiautonomous ground vehicles. *Vehicle System Dynamics*, *52*(6), 802–823. https://doi.org/10.1080/00423114.2014.902537

Gong, J., Xu, Y., Lu, C., Xiong, G. (2016). Decision-making model of overtaking behavior for automated driving on freeways. *2016 IEEE International Conference on Vehicular Electronics and Safety (Icves)* (pp. 1–6).

Gonzalez, D., Perez, J., Milanes, V., & Nashashibi, F. (2016). A review of motion planning techniques for automated vehicles. *IEEE Transactions on Intelligent Transportation Systems*, *17*(4), 1135–1145. https://doi.org/10.1109/TITS.2015.2498841

Graf, M., Speidel, O., Dietmayer, K. (2019). Trajectory planning for automated vehicles in overtaking scenarios. *2019 IEEE Intelligent Vehicles Symposium (iv)* (pp. 1653–1659).

Hu, C., & Zhao, L. (2021). Overtaking control strategy based on model predictive control with varying horizon for unmanned ground vehicle. *Proceedings of the Institution of Mechanical Engineers, Part D: Journal of Automobile Engineering*, *235*(1), 78–92.

Hu, C., Qin, Y., Cao, H., Song, X., Jiang, K., Rath, J. J., & Wei, C. (2019). Lane keeping of autonomous vehicles based on differential steering with adaptive multivariable super-twisting control. *Mechanical Systems and Signal Processing*, *125*, 330–346. https://doi.org/10.1016/j.ymssp.2018.09.011

Hu, C., Wang, Z., Qin, Y., Huang, Y., Wang, J., & Wang, R. (2020). Lane keeping control of autonomous vehicles with prescribed performance considering the rollover prevention and input saturation. *IEEE Transactions on Intelligent Transportation Systems*, *21*(7), 3091–3103. https://doi.org/10.1109/TITS.2019.2924937

Hu, L., Zhou, X., Zhang, X., Wang, F., Li, Q., & Wu, W. (2021). A review on key challenges in intelligent vehicles: Safety and driver-oriented features. *IET Intelligent Transport Systems*, *15*(9), 1093–1105. https://doi.org/10.1049/itr2.12088

Li, L., & Wang, F.-Y. (2007). *Advanced motion control and sensing for intelligent vehicles*. Springer Science & Business Media.

Li, L., Li, Y., Ni, D., & Zhang, Y. (2021). *Dynamic trajectory planning for automated lane-changing* [Paper presentation]. The 97th Annual Meeting of the Transportation Research Board, Washington, DC.

Li, W., Xie, Z., Zhao, J., Gao, J., Hu, Y., & Wong, P. K. (2021). *Human-machine shared steering control for vehicle lane keeping systems via a fuzzy observer-based event-triggered method* [Paper presentation]. IEEE Transactions on Intelligent Transportation Systems.

Li, X., Wang, W., & Roetting, M. (2019). Estimating driver's lane-change intent considering driving style and contextual traffic. *IEEE Transactions on Intelligent Transportation Systems*, *20*(9), 3258–3271. https://doi.org/10.1109/TITS.2018.2873595

Li, Y., Li, L., Ni, D., & Wang, W. (2022). Automatic lane-changing trajectory planning: From self-optimum to local-optimum. *IEEE Transactions on Intelligent Transportation Systems*, *23*(11), 21004–21014. https://doi.org/10.1109/TITS.2022.3179117

Liang, Y., Yin, Z., & Nie, L. (2021). Shared steering control for lane keeping and obstacle avoidance based on multi-objective MPC. *Sensors*, *21*(14), 4671. https://doi.org/10.3390/s21144671

Liu, W., & Li, Z. (2018). Comprehensive predictive control method for automated vehicles in dynamic traffic circumstances. *IET Intelligent Transport Systems*, *12*(10), 1455–1463. https://doi.org/10.1049/iet-its.2018.5142

Liu, W., & Li, Z. (2019). Comprehensive predictive control method for automated vehicles with delays. *IEEE Access*, *7*, 81923–81933. https://doi.org/10.1109/ACCESS.2019.2923762

Liu, W., Li, Z., Li, L., & Wang, F.-Y. (2017). Parking like a human: A direct trajectory planning solution. *IEEE Transactions on Intelligent Transportation Systems*, *18*(12), 3388–3397. https://doi.org/10.1109/TITS.2017.2687047

Luo, Y., Xiang, Y., Cao, K., & Li, K. (2016). A dynamic automated lane change maneuver based on vehicle-to-vehicle communication. *Transportation Research Part C: Emerging Technologies*, *62*, 87–102. https://doi.org/10.1016/j.trc.2015.11.011

Marcano, M., Diaz, S., Perez, J., & Irigoyen, E. (2020). A review of shared control for auto-mated vehicles: Theory and applications. *IEEE Transactions on Human-Machine Systems*, *50*(6), 475–491. https://doi.org/10.1109/THMS.2020.3017748

Marti, E., de Miguel, M. A., Garcia, F., & Perez, J. (2019). A review of sensor technologies for perception in automated driving. *IEEE Intelligent Transportation Systems Magazine*, *11*(4), 94–108. https://doi.org/10.1109/MITS.2019.2907630

Moradloo, N., Mahdinia, I., & Khattak, A. J. (2025). Who initiates the automated vehicle disengagement—humans or automated driving systems? *Journal of Intelligent Transportation Systems*, 1–18. https://doi.org/10.1080/15472450.2025.2474406

Ortega, J., Lengyel, H., & Szalay, Z. (2020). Overtaking maneuver scenario building for autonomous vehicles with prescan software. *Transportation Engineering*, *2*, 100029. https://doi.org/10.1016/j.treng.2020.100029

Paden, B., Cap, M., Yong, S. Z., Yershov, D., & Frazzoli, E. (2016). A survey of motion planning and control techniques for self-driving urban vehicles. *IEEE Transactions on Intelligent Vehicles*, *1*(1), 33–55. https://doi.org/10.1109/TIV.2016.2578706

Rasekhipour, Y., Khajepour, A., Chen, S.-K., & Litkouhi, B. (2017). A potential field-based model predictive path-planning controller for autonomous road vehicles. *IEEE Transactions on Intelligent Transportation Systems*, *18*(5), 1255–1267. https://doi.org/10.1109/TITS.2016.2604240

Stano, P., Montanaro, U., Tavernini, D., Tufo, M., Fiengo, G., Novella, L., & Sorniotti, A. (2023). Model predictive path tracking control for automated road vehicles: A review. *Annual Reviews in Control*, *55*, 194–236. https://doi.org/10.1016/j.arcontrol.2022.11.001

Suh, J., & An, S. Y. (2024). Lane change for self-driving in highly dense traffic using motion based uncertainty

propagation. *Journal of Intelligent Transportation Systems*, *28*(4), 425–442. https://doi.org/10.1080/15472450.2022.2137795

Vechione, M., & Cheu, R. L. (2022). Comparative evaluation of adaptive fuzzy inference system and adaptive neuro-fuzzy inference system for mandatory lane changing decisions on freeways. *Journal of Intelligent Transportation Systems*, *26*(6), 746–760. https://doi.org/10.1080/15472450.2021.1967153

Wang, H., Wang, Y., Zhao, X., Wang, G., Huang, H., & Zhang, J. (2019). Lane detection of curving road for structural highway with straight-curve model on vision. *IEEE Transactions on Vehicular Technology*, *68*(6), 5321–5330. https://doi.org/10.1109/TVT.2019.2913187

Wang, Q., Li, Z., & Li, L. (2014). Investigation of discretionary lane-change characteristics using next-generation simulation data sets. *Journal of Intelligent Transportation Systems*, *18*(3), 246–253. https://doi.org/10.1080/15472450.2013.810994

Wang, Z., Zha, J., & Wang, J. (2021). Autonomous vehicle trajectory following: A flatness model predictive control approach with hardware-in-the-loop verification. *IEEE Transactions on Intelligent Transportation Systems*, *22*(9), 5613–5623. https://doi.org/10.1109/TITS.2020.2987987

Xie, D.-F., Fang, Z.-Z., Jia, B., & He, Z. (2019). A data-driven lane-changing model based on deep learning. *Transportation Research Part C: Emerging Technologies*, *106*, 41–60. https://doi.org/10.1016/j.trc.2019.07.002

Xu, H., Zhang, Y., Cassandras, C. G., Li, L., & Feng, S. (2020). A bi-level cooperative driving strategy allowing lane changes. *Transportation Research Part C: Emerging Technologies*, *120*, 102773. https://doi.org/10.1016/j.trc.2020.102773

Yang, D., Zheng, S., Wen, C., Jin, P. J., & Ran, B. (2018). A dynamic lane-changing trajectory planning model for automated vehicles. *Transportation Research Part C: Emerging Technologies*, *95*, 228–247. https://doi.org/10.1016/j.trc.2018.06.007

Yang, S., Zheng, H., Wang, J., & El Kamel, A. (2021). A personalized human-like lane-changing trajectory planning method for automated driving system. *IEEE Transactions on Vehicular Technology*, *70*(7), 6399–6414. https://doi.org/10.1109/TVT.2021.3083268

Yu, H., Tseng, H. E., & Langari, R. (2018). A human-like game theory-based controller for automatic lane changing. *Transportation Research Part C: Emerging Technologies*, *88*, 140–158. https://doi.org/10.1016/j.trc.2018.01.016

Zhai, L., Wang, C., Hou, Y., & Liu, C. (2022). Mpc-based integrated control of trajectory tracking and handling stability for intelligent driving vehicle driven by four hub motor. *IEEE Transactions on Vehicular Technology*, *71*(3), 2668–2680. https://doi.org/10.1109/TVT.2022.3140240

Zhang, X., Liniger, A., & Borrelli, F. (2021). Optimization-based collision avoidance. *IEEE Transactions on Control Systems Technology*, *29*(3), 972–983. https://doi.org/10.1109/TCST.2019.2949540

Zhang, X., Zhang, W., Zhao, Y., Wang, H., Lin, F., & Cai, Y. (2022). Personalized motion planning and tracking control for autonomous vehicles obstacle avoidance. *IEEE Transactions on Vehicular Technology*, *71*(5), 4733–4747. https://doi.org/10.1109/TVT.2022.3152542

Zhang, Y., Lu, Z., Zhang, X., Xue, J.-H., & Liao, Q. (2021). Deep learning in lane marking detection: A survey. *IEEE Transactions on Intelligent Transportation Systems,* 23(7), 5976–5992.

Zhang, Y.-C. (2023). Road geometry estimation using vehicle trails: A linear mixed model approach. *Journal of Intelligent Transportation Systems*, *27*(1), 127–144. https://doi.org/10.1080/15472450.2021.1974858

Zhao, H., Lu, X., Chen, H., Liu, Q., & Gao, B. (2022). Coordinated attitude control of longitudinal, lateral and vertical tyre forces for electric vehicles based on model predictive control. *IEEE Transactions on Vehicular Technology*, *71*(3), 2550–2559. https://doi.org/10.1109/TVT.2021.3137512